ORCA – Online Research @ Cardiff

Stable Automatic Envelope Estimation for Noisy Doppler Ultrasound

J. Latham, Y. A. Hicks, *Senior Member, IEEE*, X. Yang, R. Setchi, *Senior Member, IEEE*, and T. Rainer

Abstract—Doppler ultrasound technology is widespread in clinical applications and is principally used for blood flow measurements in the heart, arteries and veins. A commonly extracted parameter is the maximum velocity envelope. However, current methods of extracting it cannot produce stable envelopes in high noise conditions. This can limit clinical and research applications using the technology. In this article, a new method of automatic envelope estimation is presented. The method can handle challenging signals with high levels of noise and variable envelope shapes. Envelopes are extracted from a Doppler spectrogram image generated directly from the Doppler audio signal, making it less device-dependent than existing image-processing methods. The method's performance is assessed using simulated pulsatile flow, a flow phantom and in-vivo ascending aortic flow measurements and is compared with three state-of-the-art methods. The proposed method is the most accurate in noisy conditions, achieving on average for phantom data with SNRs below 10 dB, a bias and standard deviation 0.7% and 3.3% lower than the next-best performing method. In addition, a new method for beat segmentation is proposed. When combined, the two proposed methods exhibited the best performance using in-vivo data, producing the least number of incorrectly segmented beats and 8.2% more correctly segmented beats than the next best performing method. The ability of the proposed methods to reliably extract timing indices for cardiac cycles across a range of signal quality is of particular significance for research and monitoring applications.

Index Terms—Maximum velocity estimation, Doppler spectrum, spectral envelope estimation, blood flow, echocardiography.

I. INTRODUCTION

Doppler ultrasound provides an accurate and noninvasive means of haemodynamic monitoring, accommodating wide diagnostic capabilities [1]. These measurements contain a wealth of information; a commonly extracted parameter is the maximum velocity envelope. The maximum velocity envelope is of particular interest in clinical applications. For example, it can be used to identify stenosis, assess its degree [2] and determine the need for a carotid endarterectomy [3]. The envelope can also be used to assess cardiac health [4] or to measure a person's cardiac output [5], providing a fast and less invasive alternative to more traditional methods [6], [7].

The maximum velocity envelope is usually estimated from a Doppler ultrasound measurement by first converting it into the time-frequency domain. The highest frequency bin containing signal at each time point can then be estimated. This gives the maximum frequency envelope (MFE). The MFE can then be converted to a maximum velocity envelope using the classic Doppler equation [1]. In the remaining document, references to envelopes will be limited to MFEs.

Obtaining clinically useful information from an MFE necessitates a skilled operator. This is both for acquiring measurements and for tracing or interpreting envelopes. A number of indices can be estimated from independent cardiac cycles within an envelope, for example, the Pulsatility index (PI) or Pourcelot's resistance index (RI) [1]. However, time restraints inherent to this currently manual process can render Doppler ultrasound monitoring impractical and prevent real-time applications. Furthermore, the process of obtaining measurements is subject to inter- and intra-observer variations [8]. These time restraints, as well as clinical benefits of averaging measurements [9]–[11] make automatic envelope estimation and beat segmentation methods highly desirable.

An automatic method for envelope estimation needs to be stable in response to variable envelope shapes, erroneous signals (such as tissue movement) and signal noise. In addition, intrinsic factors such as spectral broadening and external factors such as acquisition errors and systematic quantification make the process more challenging [12].

The majority of existing MFE estimation methods belong to two groups: integrated power spectrum (IPS) methods and image-processing methods. The former can use the Doppler audio signal directly to calculate the IPS. The maximum frequency at a time point is found by estimating the frequency bin at which signal transitions to noise. The way this point is estimated differs across the methods [12]–[17].

A recent IPS method was demonstrated to perform well [17]. This method used steps which account for spectral broadening and reject time points with poor signal quality. This method is an adapted version of the signal noise slope intersection method [12]. This modified signal noise slope intersection (MSNSI) method incorporates steps from the geometric method [16].

Image-processing methods estimate the MFE using a Doppler spectrogram image. Spectrogram images are obtained directly from the ultrasound machine [18]–[24], for example, by using video recordings. These methods extract an envelope from binary images, which are acquired by thresholding the Doppler spectrogram image and generally undergo further processing before envelope extraction. The process of thresholding differs between the image-processing methods. The selected threshold determines the amount of noise present in the resulting binary image and the difficulty of proceeding envelope extraction. The performance of these methods is

device-specific due to the images used being dependent on both user display settings and the unknown parameters used by the machine to calculate the spectrogram and show the image. In addition, they are not designed to accommodate signals with high variability in signal-to-noise ratio (SNR).

The starting positions of individual cardiac cycles are required when calculating indices such as PI or RI. Cardiac timing is generally found using an electrocardiogram (ECG), however, alternative methods which do not use ECG have been developed, for example, by applying manifold learning to ultrasound images [25], or using a tissue Doppler signal to acquire a gating signal [26]. Zolgharni et al. recently proposed an image-processing method for MFE estimation. Zolgharni's image-processing method (ZIPM) was shown to perform well. This method also includes a process of beat segmentation that does not require an ECG signal [24]. It operates by detecting local minima immediately before and after systolic peaks. However, this assumption regarding MFE shape may not hold true in cases of poor signal quality and low SNRs.

The present lack of an automatic method capable of extracting stable envelopes over extended periods of time, especially when used with low SNR measurements, is the principal motivation for the presented work. This work introduces a new fully automatic MFE estimation method and a new beat segmentation method. The proposed method for beat segmentation has been developed to function using solely the extracted MFE, removing the need for additional hardware such as ECG. Furthermore, it relaxes the assumptions concerning the shape of the extracted MFE in comparison to [24], which improves its reliability in cases of irregularly shaped MFEs.

The proposed MFE estimation method, the Otsu morphological method (OMM), is based on image-processing techniques. However, it uses Doppler spectrogram images generated directly from the Doppler audio signal, rather than using the Doppler spectrogram images displayed by the machine. Such an approach enables processed images to be explicitly defined within the OMM method, thus ensuring image consistency and removing uncertainty regarding their design. The novelty of the proposed method is twofold. First, its ability to define and vary Doppler spectrogram image parameters enable identification of effective threshold values, as explained in detail in Section II-C. Second, OMM operates dynamically with respect to SNR by applying morphological operations in a hierarchical manner. As a result, the OMM method can extract highly stable envelopes from a wide range of signal qualities.

The accuracy of the proposed MFE estimation method is compared to three other methods: two IPS methods (MSNSI and the modified geometric method (MGM) [15]) and one image-processing method (ZIPM). In the case of simulated and phantom data, the true MFE is known. This enables evaluation of the proposed method using standard deviation (STD), bias and correlation statistics. Through the addition of noise to these data sets, the MFE estimation methods are evaluated across a range of SNR values. The OMM method is shown to be the most stable in noisy measurements.

The ability of each MFE estimation method to produce envelopes suitable for monitoring applications is also evaluated. Each MFE method is used to extract envelopes from in-vivo data. The proposed method of beat segmentation is then applied to each envelope, and the percentage of beats correctly segmented in each case is found. The combination of the proposed MFE estimation and beat segmentation methods resulted in 8.2% more beats correctly segmented than the next best performing method.

To conclude, the main contributions of this work include:
- a method for extracting stable MFEs from low quality Doppler audio signals (Section II);
- a method of beat segmentation using only the MFE (Section III); and
- a comparison between the performance of the proposed MFE estimation method with the MSNSI, MGM and ZIPM methods. Comparisons are facilitated using simulated pulsatile Doppler data, phantom data and over 2 hours of in-vivo data (Section IV).

II. PROPOSED MFE ESTIMATION METHOD

This section describes the proposed MFE estimation method. The method consists of three main parts: signal preparation, binary image generation, and hierarchical morphological filtering (Fig. 1). The proposed method uses the Otsu algorithm [27] to generate binary images, followed by morphological filtering. OMM uses directional Doppler audio signals; Fig. 2 provides a simple example of how these are generated within a Doppler device [1].
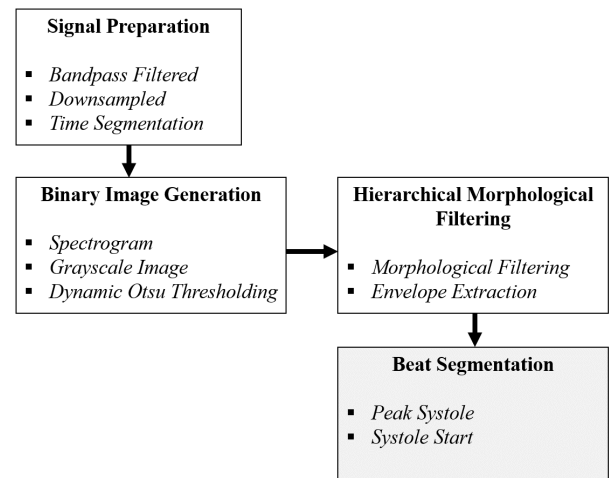
Fig. 1. OMM envelope extraction and beat segmentation stages.

A. Signal Preparation

The Doppler audio signal is first processed to remove unwanted signals and make the following operations more time-efficient.

A high-pass filter (or 'wall-thump filter') is used to remove extrinsic low-frequency components arising, for example, from vessel walls [28]. A typical cut-off frequency of 200 Hz is used [29]–[31], which preserves the frequencies of interest. A low-pass filter is applied to remove high frequencies greater than those of interest. A cut-off frequency of 8kHz is used for recorded data in the presented work. The filtered audio is finally downsampled to 16 kHz (allowing the full frequency

Fig. 2. Block-diagram of simple continuous wave Doppler system.

range of the filtered audio to be analysed), which removes noise and speeds up the remaining operations. The above procedures should be implemented with consideration of the velocities being measured and the hardware used.

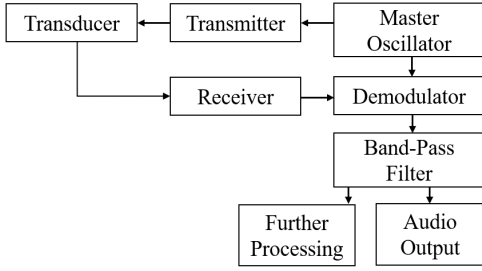### B. Image Generation and Enhancement

The proposed method uses an image created from a spectrogram calculated using the Doppler audio signal. This means that parameters values can be explicitly defined, giving full control over characteristics of the images generated and used. Such an approach contrasts favourably with capturing an image from a machine, where the image generation process and parameter values used are unknown.

The spectrogram is calculated using the short-term Fourier transform (STFT) of the recorded Doppler audio signal. A 10 ms Hamming window ($W = 10$ ms) is used, with 50% overlap. Using zero padding, a 512-point FFT is calculated. The chosen values ensure that changes in blood velocity are captured [1] and facilitate the application of fine morphological operations to the binary image in the following stage. This process produces pixels with 5 ms and 31.5 Hz time and frequency resolution respectively in the Doppler spectrogram images. Further processing of spectrogram images are affected by this time-frequency pixel resolution; to reflect this, this resolution should be replicated when implementing the proposed method.

The resulting matrix of STFT values is converted into decibels with a dynamic range of 60 dB, set with respect to the maximum value in the matrix. This wide range ensures the signal, which can change in intensity, is captured each time.

The matrix is converted into a grayscale image. To aid envelope estimation, high-frequency noise can now be removed using a Gaussian filter [32]. This has been implemented using a 5 x 5 Gaussian kernel in line with previous research [21], [33]. Whilst the previous works do not disclose pixel resolution, in this article a 5 x 5 Gaussian kernel is equivalent to 25 ms by 158 Hz. With respect to these previous works, a smaller standard deviation of 1 has been used to preserve more rapid fluctuations in blood flow. Fig. 4a and Fig. 4b provides an example of the spectrogram and final image.

C. Dynamic Threshold Identification

In this stage, the grayscale image is converted to a binary image by applying a threshold. The purpose of this operation is to separate signal from noise, with the aim of setting all image pixels corresponding to noise to the value of zero and

setting all image pixels corresponding to signal to the value of one.

A suitable threshold is identified using the Otsu method [27], which assumes a histogram with bimodal distribution (i.e., signal and noise), and calculates the value which best divides these distributions. This process identifies an optimal threshold using a sequential search, during which the success of each threshold is quantified using Otsu's objective criterion (η). The threshold with the maximum η value is selected. This maximum η value is referred to as the effectiveness metric (EM).

However, the transition point between signal and noise can be masked in low SNR conditions. To detect this point effectively, a range of images is generated for a variety of window lengths (W). In each case, a threshold and corresponding EM value is calculated using the Otsu method. The values of EM indicate how well an image has been separated into two classes. The W that is most effective at separating the signal from the noise is determined by both SNR and Doppler profile.

Consequently, the best threshold is identified as that which corresponds to the largest EM value. This threshold is then applied to the image generated using the standard $W = 10$ ms. This gives a well thresholded binary image with the specific time and frequency resolution defined in the previous section. This binary image is cropped to remove frequency bins below 200 Hz in response to the high-pass filter described in Section II-A.

In the presented work, 10 window lengths varying linearly from $W = 1$ ms to $W = 0.1$ s were used. This range was chosen empirically, as the best window was found to very rarely exceed it. EM is calculated using the following equation:

$$EM_i = \frac{max(\sigma_{Bi}^2)}{\sigma_{Ti}^2} \tag{1}$$

where i varies between 1 and 10 and corresponds to index of window length, σ_B^2 and σ_T^2 are the between-class and total variance within the image [27].
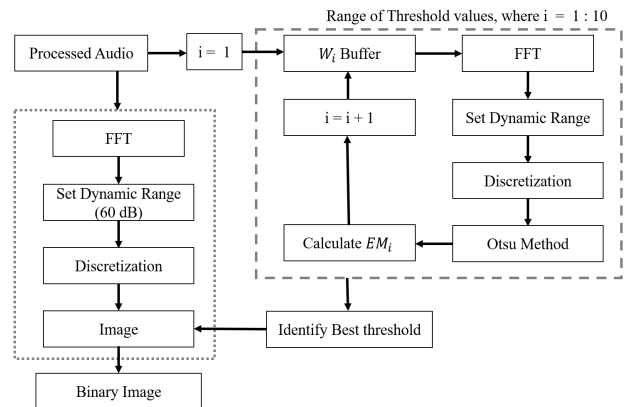

Fig. 3. Dynamic threshold selection, using variable window lengths (W_i).

D. Hierarchical Morphological Filtering

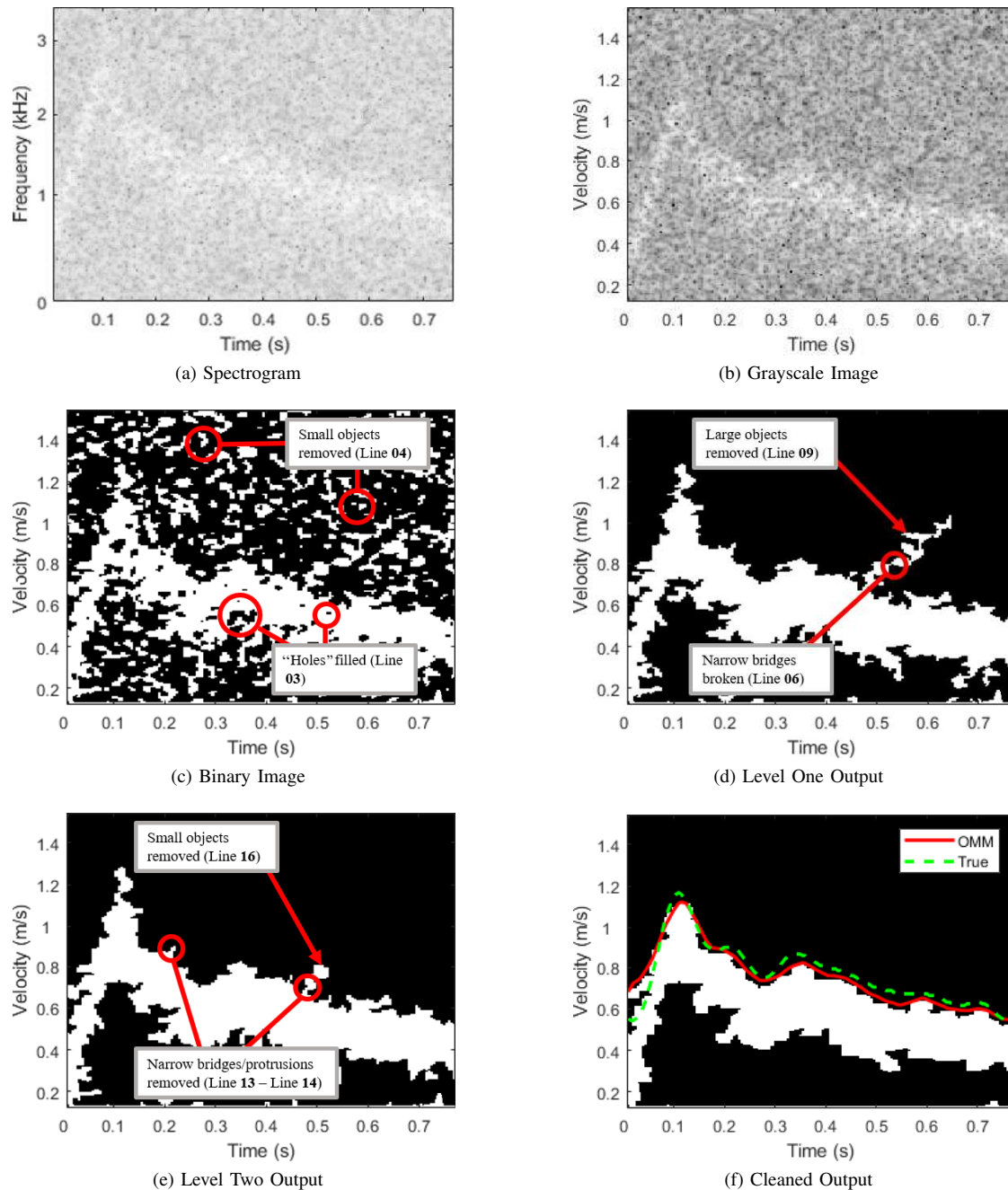The binary image can now be processed and used to estimate the MFE.

Fig. 4. Image stages within OMM, using a simulated common carotid Doppler signal with estimated SNR of -3 dB. Equivalent row velocity is displayed for images 4b to 4f. Extracted OMM envelope and reference true velocity is displayed in 4f. Pixels have a time and frequency resolution of 5ms and 31 Hz, respectively.

An example of the binary image at this stage is displayed in Fig. 4c. This example illustrates how in low SNR conditions, the threshold is unable to fully isolate the signal. Noise, which has been incorrectly identified as signal, will be referred to as noise. In higher SNR conditions, the threshold is better able to isolate the signal producing images more similar to those displayed in Fig. 4d to 4f. To account for the variability in SNR, morphological operations are applied in a hierarchical manner. This prevents images with high SNRs being subject to unnecessary processing. This algorithm is illustrated using pseudocode in Fig. 5.

The binary image is passed to level 1 and possibly level 2 of the algorithm if more than one object is present in the image, i.e., the SNR of the image is low. Objects are defined as clusters of multiple pixels with non-zero values (white pixels) connected either vertically, horizontally or diagonally. Lower SNRs result in more objects and so corresponding binary images undergo further processing. Fig. 5 illustrates that a number of operations are repeated. These will now be briefly discussed.

Initially, the number of objects is reduced to prevent unnecessary further processing. This is done by setting pixels

```
[01]        Set First Row To 1
[02]        if # Objects > 1 % Level 1
[03]            Fill Image
[04]            Remove Islands < 300
[05]            if # Objects > 1 % Level 2
[06]                Open Image % vertical line structuring element, length 3
[07]                Set First Row To 1
[08]                Fill Image
[09]                Remove Islands < 500
[10]            end
[11]        end

            % Clean Image

[12]        Fill Image
[13]        Open Image % vertical line structuring element, length 5
[14]        Open Image % horizontal line structuring element, length 5
[15]        Set First Row To 1
[16]        Remove Islands < 100
```

Fig. 5. Pseudocode of the proposed algorithm for hierarchical morphological filtering to extract MFE from binary image.

contained in the lowest frequency row to 1. This is done on line **[01]** and repeated if necessary on lines **[07]** and **[15]**. This is effective at retaining small low-frequency objects, which otherwise would be removed in proceeding steps, for example, within the diastolic portion of Fig. 11. This condition, however, does assume that flow is present in the first frequency bin.

Next, the signal regions are strengthened using a flood-fill operation. Objects attributed to noise tend to be smaller, and less homogeneous than those reflective of signal. However, the signal portions can contain "holes" (as illustrated in Fig. 4c). This operation is performed on lines **[03]** and if necessary on line **[08]** and on line **[12]**.

After strengthening the signal, any object with an area smaller than 300 pixels is considered to be noise and is removed in level 1 (line **[04]**), as illustrated in Fig. 4d. If the image is passed to level 2, the operation is repeated on line **[09]**. Remaining noise at this stage is often contained in larger objects, due to the lower SNR of the images reaching this level, and so an area of 500 is used in level 2 (comparison between Fig. 4d and Fig. 4e illustrates this). The final area used in the cleaning stage is 100 on line **[16]**. This assumes little noise and removes small isolated objects, which appeared as a result of opening operations. The choices of these area sizes were guided by previous works and determined through empirical investigation, previous works have used clusters ranging from 50 [23] to 500 [24], however, the pixel resolutions in these cases are not explicitly defined.

Additionally, in level 1 and in the cleaning stage, opening operations are used to break small horizontal and vertical connections respectively. This is done prior to the removal of objects, on lines **[13]**, **[14]** and **[06]**. This isolates weakly connected objects or small protrusions (as illustrated in Fig. 4e), reduces noise and smooths the image prior to envelope estimation.

The resulting image can now be used to extract the MFE. The MFE is found for each time point separately, using the column of pixels associated with that time point. The maximum frequency within each column is taken as the white pixel (pixel representative of signal) which is next to the largest number of consecutive black pixels. This is similar to the biggest-gap method, which includes weightings applied

to each group of noise pixels based on frequency [21]. The envelope is then smoothed using a 10-point moving average filter. The unsmoothed envelope is also retained for further steps described in Section III. The extracted OMM envelope and reference true velocity is displayed in Fig. 4f.

In cases where both forward and reverse flow is of interest, the steps described to extract the MFE are repeated for the positive and negative Doppler shifts respectively. This gives an MFE for forward and reverse flow, and an overall MFE can then be found by taking the absolute maximum of each MFE at each time point.

III. BEAT SEGMENTATION METHOD

A number of clinically valuable blood-flow variables can be extracted from the MFE; these usually require the envelope to be segmented into individual cardiac cycles. Such variables are discussed further in Section IV-F. Averaging or monitoring these variables requires a number of beats to be segmented. In other scenarios, such as research applications, thousands of cardiac cycles may need to be segmented. This can be very challenging without an automatic means of beat segmentation.

In this section, an automatic method of segmenting the MFE into individual cardiac cycles is presented. This is achieved by finding the approximate starting locations of systole. Systole is the phase of the cardiac cycle whereby the heart contracts, resulting in blood being pumped out of the heart. The peak of systole is the maximum blood velocity during this phase and is assumed to be the maximum frequency of the MFE during a cardiac cycle.

The two main steps in the proposed beat segmentation method is the identification of peak systole positions, and subsequently, identification of the systole start positions. The method uses a similar approach to a previously described method of beat segmentation [34]; specifically using a low-pass filtered MFE to find temporal indices and using the rising slope of systole to estimate the start of systole. However, the original method could not be implemented as the relevant document was limited to high-level details.

The proposed approach allows the start of systole to be identified, even for MFEs which exhibit unusual behaviour either side of peak systole. This overcomes limitations of assuming that a minima occurs prior to the start of systole [24]. The method requires only the MFE as an input, in the given work segmented envelopes are 4s long.

A. Peak Systole Identification

Peak systole positions are first approximated using the unsmoothed MFE (described in Section II-D). The mean of this envelope is first set to zero, and then it is low-pass filtered (LPF), which removes frequencies above 3.7 Hz, and results in a signal which is more sinusoidal in appearance. This assumes a heart rate of less than 220 BPM, which is well within the normal range for adolescents and adults [35].

The approximate peak systole positions are then found by identifying peaks in the sinusoidal signal. A "minimum peak distance" condition is used to make this more reliable (i.e., time between consecutive peaks). A minimum peak distance
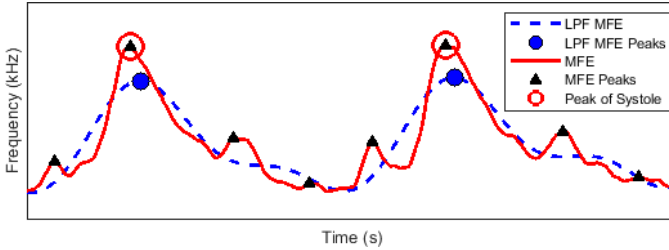
Fig. 6. Peak systole identification using approximate peaks found from the LPF MFE, illustrated for scenario where MFE contains numerous peaks, for example, due to low SNR conditions.

of $0.8/f_{HR}$ is used, where f_{HR} is the estimated heart rate frequency. This condition assumes that heart rate reduces no more than 20% within a processed envelope.

The heart rate frequency is estimated from the power spectral density (PSD) of the sinusoidal signal, calculated using the Welch method. The frequency corresponding to the maximum value in the PSD is taken as f_{HR}. Final peak systole positions are taken as the peaks in the (smoothed) MFE closest in time to the approximate positions. Fig. 6 illustrates how peaks found in the LPF MFE are used to identify peak systole in the MFE.

B. Start of Systole Identification

The next step is to estimate the start of systole. Low-frequency content in the Doppler audio signal can obscure the transition between diastolic and systolic blood flow (Fig. 7) and thus prevent the start of systole positions from being easily identified.

To overcome this, the rising slope of systole is used. This occurs immediately prior to peak systole. The gradient of this slope is used to plot a line that intersects 0 Hz. This point is taken as the approximate start of systole. Two points are selected on the rising slope to calculate the gradient and to plot the intersection line. The two points correspond to 50% and 80% of peak systole (the locations of which were found in Section III-A). These percentages were empirically chosen as this region of the envelope typically exhibits a strong signal. Fig. 7 also illustrates how this approach can be implemented
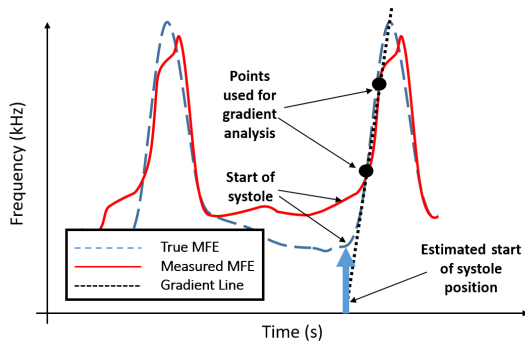

Fig. 7. Method of estimating start of systole, illustrated for scenario where start of systole and peak systole are obscured, for example, due to low SNR conditions.

in scenarios where the peak of systole is not clearly defined, for example, in poor SNR conditions.

IV. EVALUATION METHODS

The performance of the proposed method has been quantitatively assessed using simulation data, phantom data and in-vivo data; these datasets are described in Sections IV-D, IV-E and IV-F, respectively. The performance of OMM is compared to that of three other MFE estimation methods. The MFE methods chosen to provide comparison are two IPS methods and one image-processing method; the implementation of these methods is described in Sections IV-B and IV-C respectively.

The IPS methods chosen to offer comparison are the MSNSI and MGM methods. MSNSI has been selected as it is focused on envelope estimation as opposed to maximum frequency estimation at specific time points and was shown to perform well [17]. MGM is an older IPS method [15], which has been shown to be reasonably stable in varying SNR. This is used to provide a further comparison with IPS methods. The image-processing method chosen to offer comparison is ZIPM [24]. ZIPM was selected due to it being a recent method, which demonstrated good correlation with expert tracings. Furthermore, ZIPM is designed for fully automatic tracing (as OMM is) and for aortic Doppler measurements, which are used for in-vivo testing in this study.

The performance of IPS methods has typically been validated using a combination of simulated data, phantom data, and in-vivo data. Popular simulation approaches model simple constant flow conditions using Gaussian processes to represent Doppler signals [36]–[38]. For this study, pulsatile flow has been simulated. In the case of phantom and simulated data, the true maximum velocity is known. This allows MFE estimation methods to be quantitatively assessed using statistical measurements; bias and standard deviation are commonly used [12]–[17] and have been implemented in this study. Correlation statistics have also been calculated for these data sets; they provide a measure of the similarity between the extracted MFEs and the true envelope shape. This is included as good correlation is essential for reliable beat segmentation and provides further evaluation with regards to the stability of extracted envelopes.

Image-processing methods have been previously assessed using in-vivo data and thus have not included evaluation with respect to different levels of SNR. Instead, such assessments are based on comparisons made with expertly traced envelopes. Here, we assess an image-processing method using simulated and phantom images; this allows for a quantitative evaluation. The addition of Gaussian noise to signals enable different SNR values to be investigated. This technique has been used with the phantom and simulated datasets, allowing the performance of each MFE estimation method to be assessed with respect to diminishing signal quality.

In-vivo data has been used in the current study to investigate the ability of each MFE estimation method to produce MFEs suitable for beat segmentation. MFEs are extracted using each evaluated method and processed using the proposed

means of beat segmentation. The percentage of beats correctly segmented for each of these traces is then analysed. In the case of long continuous measurements, such as the in-vivo data (Section IV-F), audio has been processed in 4-second segments.

All processing has been performed using MATLAB R2018a (The Mathworks, Inc., Natick, MA, USA).

A. OMM Method Implementation

The OMM method has been implemented as described in Section II. Threshold and associated *EM*s have been calculated using the image-processing toolbox in Matlab.

In cases where both forward and reverse flow is of interest (such as the simulated data displayed in Fig. 11), the envelopes for the positive and negative flow are calculated separately. These two envelopes are used to generate the final MFE. At each time point, the positive and negative maximum frequencies are compared, and the maximum absolute frequency is used for the final MFE.

B. IPS Method Implementation

The performance of the MGM [15] and MSNSI [17] methods has been assessed and compared to that of the OMM method. These have been implemented as described in their publications.

C. ZIPM Implementation

The ZIPM method uses images acquired from an ultrasound machine by a frame grabber. In the presented study, the images used were generated using an approach similar to generating images within OMM, as described in Section II. The method differed from OMM by using a dynamic range of 20 dB for the phantom and simulation data, and 40 dB for the in-vivo data.

It was found that varying the dynamic range in this way was necessary to achieve good results across the datasets. These dynamic ranges were chosen by testing values from 15 to 60 dB, and choosing the best value in terms of STD and bias for the simulation and phantom data (with no added noise), and visually inspecting envelopes produced for in-vivo data. The images were then resized to be more representative of those described in the article [24].

In cases where both positive and negative flow is of interest, the approach implemented by OMM is used (Section IV-A). An example of an image generated using this approach is displayed in Fig. 8.

D. Simulation Data

The performance of MFE estimation methods has previously been investigated using simulated data [14]–[17], [37] and [38]. The advantage of using simulations is that the true maximum frequency associated with the modelled scatterers is known. These models have predominantly simulated simple flow conditions, representing steady flow. Such models allow the process to be simplified; however, they limit how realistic resulting data is, for example, they do not take into account
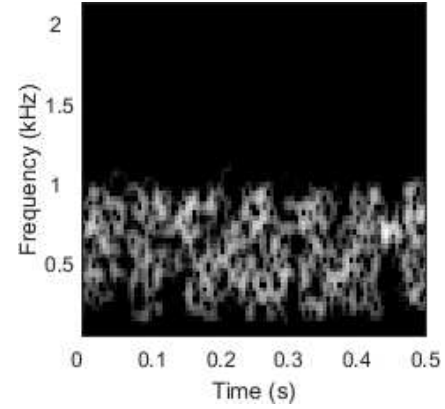

Fig. 8. Image with dynamic range of 20 dB, generated for ZIPM implementation using Phantom data.

ultrasound device parameters such as sample volume (SV) and do not represent realistic pulsatile blood flows. The simulated data used within this study represents pulsatile flow and is generated using numeric ultrasound simulation. This approach results in raw data similar to that measured by an ultrasound machine, allowing MFE estimation performance to be rigorously tested on very realistic data.

The software Field II, developed by Jensen [39], [40], has been used to simulate realistic flow data. It has been well validated and used extensively for ultrasound research, including the use of simulations to accurately obtain velocity estimates [41]–[43].

In this study, the software was used to generate raw data for pulsed-wave ultrasound interrogating pulsatile flow using insonation angles of $30°$ and $60°$. In pulsatile flow, the velocity profile changes as a function of time. A waveform representative of flow from a given artery can be synthesised using its Fourier components [1]. Using the Womersley model [44], realistic flow profiles can be generated.

These time-dependent profiles allow the position of the modelled scatterers to change between ultrasound pulses, thus simulating pulsatile flow. The contributions from all scatterers traversing the SV allow the Doppler spectrum to be formed. A range-gate was used to simulate a SV, which is positioned at the centre of the lumen and spans its width. An online example was used as a reference to generate a model using a linear array transducer [45].

The settings used to generate the model are displayed in Table I. These were used to generate simulated data for one complete cardiac cycle, for femoral and common carotid artery flows. An example of simulated data for the femoral artery is presented in Fig. 11.

Bias and STD statistics are calculated for the simulated data. These statistics are used to contrast the performance of the tested MFE estimation methods and are calculated using the estimation error at each time point within the MFE [17]. The correlation coefficient of an estimated envelope and the true velocity envelope can also be calculated, providing a numerical measure of the similarity between the two waveforms. These statistics are calculated for the simulated femoral artery data.

In addition to the above performance metrics, waveform

indices can be calculated from extracted envelopes and compared to their true values. These indices use minimum and end-diastolic velocity values. Due to the end-diastolic value for the femoral artery being very close to 0 and some MFE methods tending towards 0 in poor noise conditions, simulated data of the carotid artery is used to compare the estimation of these indices.

TABLE I
PARAMETERS USED WITHIN FIELD II TO SIMULATE FLOW

Parameter	Value
Scatterer Settings	
Heart Rate	90 bpm (Femoral)
	80 bpm (Carotid)
Lumen Radius	4 mm
Lumen Centre Depth	40 mm
X-range	40 mm
Y-range	8.8 mm
Z-range	8.8 mm
Number of Scatterers	67,851
Peak Velocity	1 m/s (Femoral)
	1.2 m/s (Carotid)
Insonation Angle	30°, 60°
Linear Array Transducer Settings	
Speed of Sound	1540 m/s
Centre Frequency	2 MHz
Sampling Frequency	100 MHz
Element Lateral Width	0.39 mm
Element Elevation Height	5 mm
Kerf	0.05 mm
Element Pitch	0.44 mm
Pulse Repetition Frequency	8 kHz
Excitation Pulse	Sinusoid
Number of Elements	64
Cycles in Emitted Pulse	10
Focus vector (Transmit and Return)	[0 0 40] mm

E. Phantom Data

Phantom data was collected using a Gammex optimiser 1425A (Gammex Inc., USA). This is a self-contained system, which is capable of generating steady laminar flow rates from 1.7 to 12.5 ml/s. The system is designed for testing aspects of ultrasound device performance, including the accuracy of measured flow rates. The 1425A uses structures which are ultrasonically similar to human tissue ensuring a realistic platform for research. The embedded vessel can be scanned using an insonation angle of 50°, and has an inner diameter of 4 mm. Data was collected from the phantom using a Toshiba TUS-A500 diagnostic ultrasound system. A 3 MHz probe was used to measure steady flow across the embedded vessel through pulsed-wave ultrasound. An audio output on the machine was employed to record the directional Doppler audio on a laptop, using 44.1 kHz sample rate, and 16-bit depth.

Typical peak blood velocities within the ascending aorta are of the order of 0.7 m/s, but varies between patients [46]. To reflect typical flowrates, data was measured using flowrates of 0.4, 0.8 and 1 m/s; 10 seconds of data was recorded for each flow rate. As with the simulation data, bias and STD statistics were calculated; these were calculated using 1s segments of data and then averaged. An example of data measured using the Phantom is displayed in Fig. 15.

F. In-Vivo Data

The MFE estimation methods were further evaluated using in-vivo data, an example of in-vivo data is displayed in Fig. 16. Data was collected from 11 healthy adult volunteers using an ultrasonic cardiac output monitor (USCOM) 1A ultrasound device (USCOM, Sydney, Australia). This is a continuous-wave ultrasound device, which operates at 2.2 MHz and is used in clinical applications to measure and monitor cardiac health indicators, including cardiac output. Positive-flow Doppler audio was recorded on a laptop. The audio was sampled from the device using a 44.1 kHz sample rate and 16-bit depth. Proper ethical permission was attained from the School of Engineering Ethics Committee (Cardiff University) and signed consent was obtained from each volunteer. Data was collected from the suprasternal notch, giving measurements of blood flow across the aortic valve. The participants were in the supine position. The data consists of 229 recordings, totalling over 2 hours of audio. Using (2), the in-vivo SNR ranges from approximately 10 dB to 30 dB.

The true MFEs under these conditions are unknown, meaning performance cannot be investigated using STD, bias or correlation statistics. Instead, in-vivo data has been used to evaluate how well each MFE method produces envelopes suitable for accurate beat segmentation. The proposed beat segmentation method is used to segment envelopes, extracted using each MFE method, into individual cardiac cycles. The success of each MFE estimation method to produce MFEs suitable for this purpose can then be evaluated. This is done through comparing the percentage of total beats segmented from all of the recordings with the number of false positives, false negatives and true positives associated with a sample of the in-vivo data. These data contain scans exhibiting a range of quality allowing a more realistic investigation of performance with respect to real-world measurements.

G. Evaluation of Performance in Varying SNR

The performance of estimated envelopes has been assessed in response to varying SNR. This has been achieved by adding noise to the simulated and phantom datasets. SNR is estimated from the spectrogram using the following relationship [17]:

$$SNR(dB) = 10log_{10}\left(\frac{\hat{P}_S - \hat{P}_N}{\hat{P}_N}\right) \qquad (2)$$

where $\hat{P}_s$ is the mean power contained in the entire spectrogram, and $\hat{P}_N$ is the mean power of a region of the spectrogram which contains only noise. This region is identified as a range of bins which exceed the estimated MFE [17]. In the case of phantom and simulated data the true MFE is known, this enables all bins reflective of noise to be used when calculating $\hat{P}_N$.

V. RESULTS

The performance of the four MFE estimation methods has been systematically evaluated using the datasets described in Section IV. The results from this analysis are now presented.
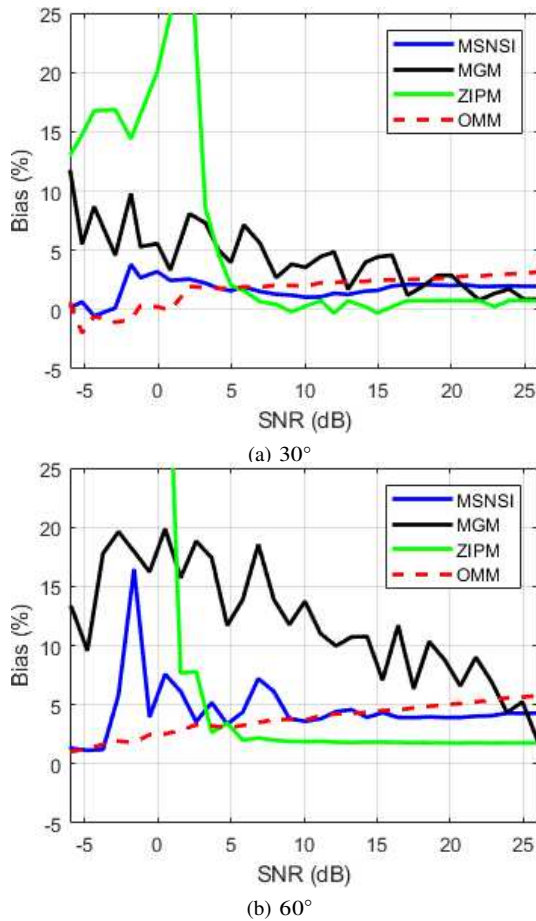
(a) 30°

(b) 60°

Fig. 9. Bias statistics for simulated femoral artery data using insonation angles of 30° and 60° across a range of SNR values.

(a) 30°

(b) 60°

Fig. 10. STD statistics for simulated femoral artery data using insonation angles of 30° and 60° across a range of SNR values.

A. Simulation Results

The performance of the MFE estimation methods has been assessed using the simulated pulsatile flow data. An example of this data is displayed in Fig. 11.

Statistics for the simulated data have been acquired at SNR values from -6 dB to 26 dB in steps of 1 dB; this was repeated three times and averaged. The calculated bias and STD of normalised maximum velocity for each method is displayed in Fig. 9 and Fig. 10, respectively. These have been calculated using absolute envelope values, which prevents bias tending towards zero when an MFE estimation method tends towards zero in low SNR.

At SNRs greater than approximately 5 dB, ZIPM achieved the lowest bias. At SNRs below this, OMM achieved the lowest bias values. OMM achieved the most consistent STD values across the SNR range and the lowest values below 10 dB. Above 10 dB, MSNSI achieved the lowest STD values of approximately 2%.

The correlation coefficient between each method and the true envelope across the investigated range of SNR values is displayed in Fig. 12. This illustrates how similar the extracted envelope is to the true velocity envelope and the effect SNR and insonation angle has on this quality.

Fig. 12 demonstrates that overall OMM produces an MFE very similar to the true MFE and remains stable for signals

with low SNR values. For both cases of insonation angle, OMM achieved a correlation of greater than 95% at -6 dB. Fig. 12 is consistent with visual inspections of the extracted MFEs, which demonstrate the OMM envelopes remaining highly stable and consistent across the SNR range, with the envelopes produced by the remaining methods becoming increasingly

Fig. 11. Simulated femoral artery using insonation angle of 30°, unfiltered with added noise to give SNR of 10 dB. Displayed with corresponding MSNSI, OMM and true velocity envelopes. Spectrogram image displayed using 60 dB dynamic range.

(a) 30°

(b) 60°

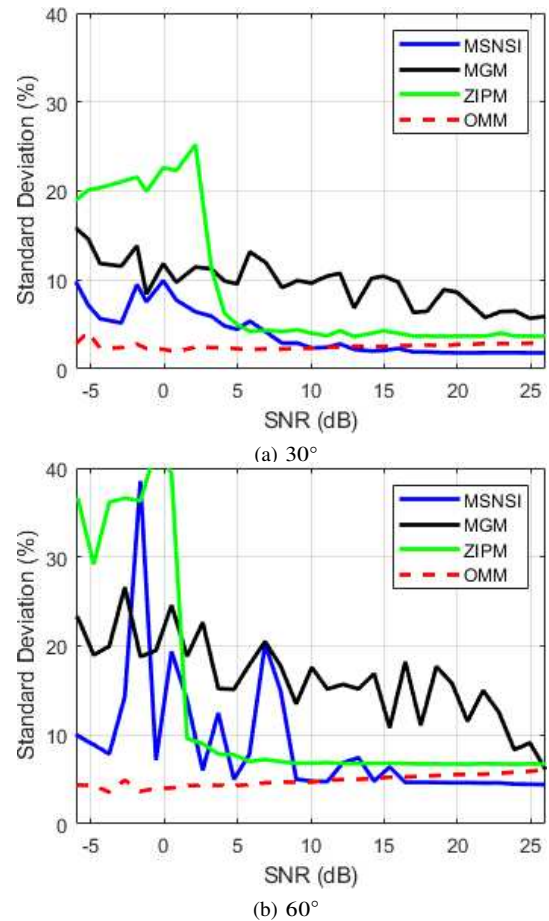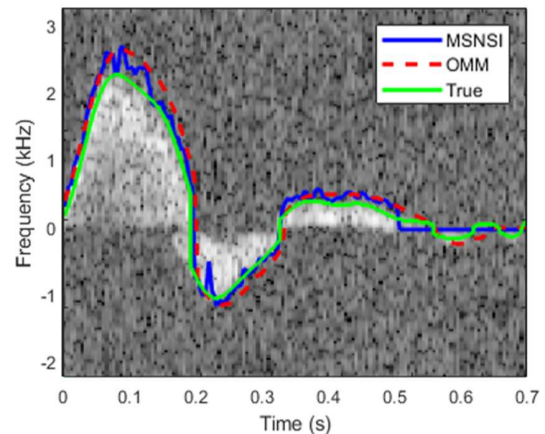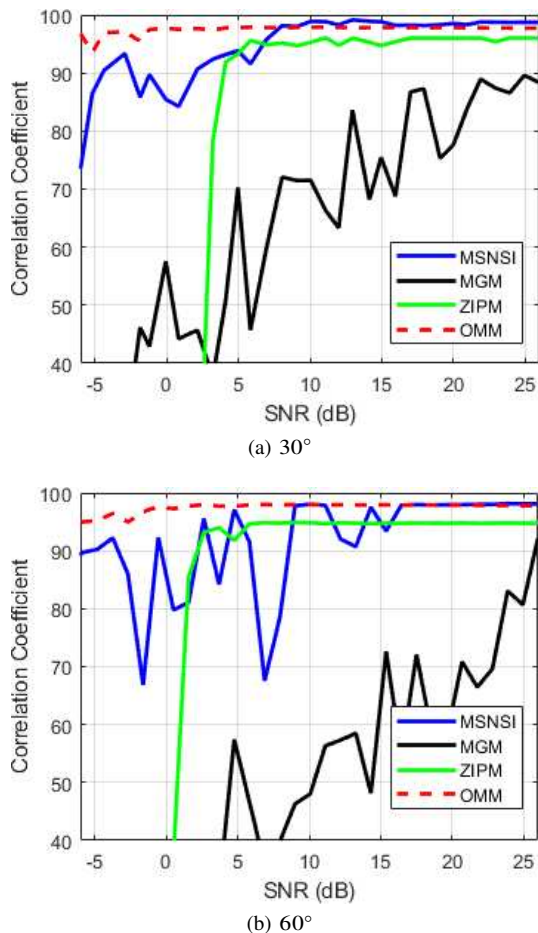Fig. 12. Correlation statistics for simulated femoral artery data using insonation angles of 30° and 60° across a range of SNR values.

erratic at SNRs decreasing below approximately 6 dB. This is particularly true for the IPS methods in the 60° simulation data.

PI and RI indices were calculated for the simulated carotid artery data using (3) and (4). PI describes the degree of damping at different arterial sites, and RI is an indicator of circulatory resistance beyond the measurement point [1].

$$PI = \frac{S - D_{min}}{M} \tag{3}$$

$$RI = \frac{S - D_{end}}{S} \tag{4}$$

where S is the maximum velocity, D_{min} is the minimum velocity, D_{end} is the velocity at the end of diastole and M is the average velocity; this is illustrated in Fig. 13. These values are calculated from estimated MFEs using the true cardiac timing indices, i.e., S is the maximum velocity during systole and D_{min} and D_{end} is the minimum and end velocity respectively during diastole.

Such indices are based on ratios attained from the MFE, and so are less prone to certain errors such as incorrect insonation angle measurement [1]. The calculated RI and PI indices are displayed in Fig. 14.

OMM achieved the best overall RI percentage error. Above approximately 5 dB, ZIPM and OMM achieved similar results.
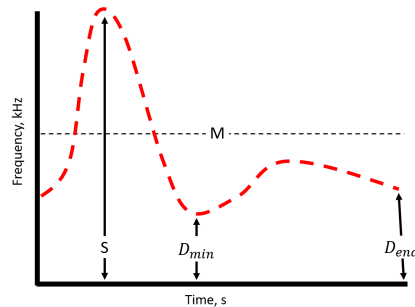

Fig. 13. Values used to compute RI and PI indices.

At high SNRs, ZIPM achieved the lowest PI error of –3.7%, with OMM and MSNSI achieving similar absolute errors for the 30° data (OMM with -6.5%, and MSNSI with 6.3%). Increasing the insonation angle to 60° resulted in OMM decreasing to -10%, and MSNSI increasing to 18% at high SNRs. ZIPM was less effected, reducing to -4.3%.

B. Phantom Results

The calculated bias and STD statistics are displayed in Table II for the velocities and SNR ranges investigated using the phantom data. The OMM method consistently resulted in the lowest STD, illustrating the stability of extracted MFEs using this method. No methods consistently performed best with respect to bias measurements. However, with respect to data with SNRs below 10 dB, OMM on average displayed the best performance. Comparing OMMs bias and STD with those from the best performing alternative method at each SNR below 10 dB, on average OMM achieves a bias and STD 0.7 % and 3.3 % lower, respectively. An example of the recorded sample data and associated OMM and MSNSI MFEs are illustrated in Fig. 15.

TABLE II
BIAS AND STANDARD DEVIATION STATISTICS FOR DIFFERENT ENVELOPE ESTIMATION METHODS, USING PHANTOM DATA

| SNR (dB)	Bias (%)				STD (%)			
	OMM	MSNSI	MGM	ZIPM	OMM	MSNSI	MGM	ZIPM
Constant Flow Velocity of 0.4 m/s								
0	-0.7	3.5	3.7	28.0	0.5	5.0	9.8	8.9
3	0.1	2.0	1.2	28.3	0.4	3.2	4.7	8.3
5	-0.3	1.4	0.5	31.3	0.3	2.1	3.1	8.2
10	0.6	0.9	0.1	2.8	0.3	1.4	1.8	1.3
14	1.3	0.9	0.2	2.2	0.3	1.1	1.7	0.8
Constant Flow Velocity of 0.8 m/s								
0	0.3	3.3	1.1	17.1	0.6	4.9	8.0	10.4
3	0.8	2.5	-0.1	14.7	0.5	4.7	4.8	9.4
5	1.2	1.3	-0.4	21	0.6	4.0	3.1	7.4
10	1.7	1.0	-0.3	4.9	0.5	2.4	2.3	2.2
13	2.2	1.1	-0.3	3.3	0.5	1.9	2.3	0.9
Constant Flow Velocity of 1 m/s								
0	-0.8	2.5	-0.7	8.5	1.0	5.4	7.4	11.1
3	0.1	1.2	-1.8	14.3	0.8	3.7	4.1	8.2
5	0.4	0.8	-1.8	18.4	0.6	2.9	3.3	6.6
10	1.3	0.5	-1.8	4.6	0.5	1.7	2.7	1.7
14	1.4	0.3	-1.7	3.2	0.4	1.2	2.4	0.8

(a) 30°   (b) 60°

(c) 30°   (d) 60°
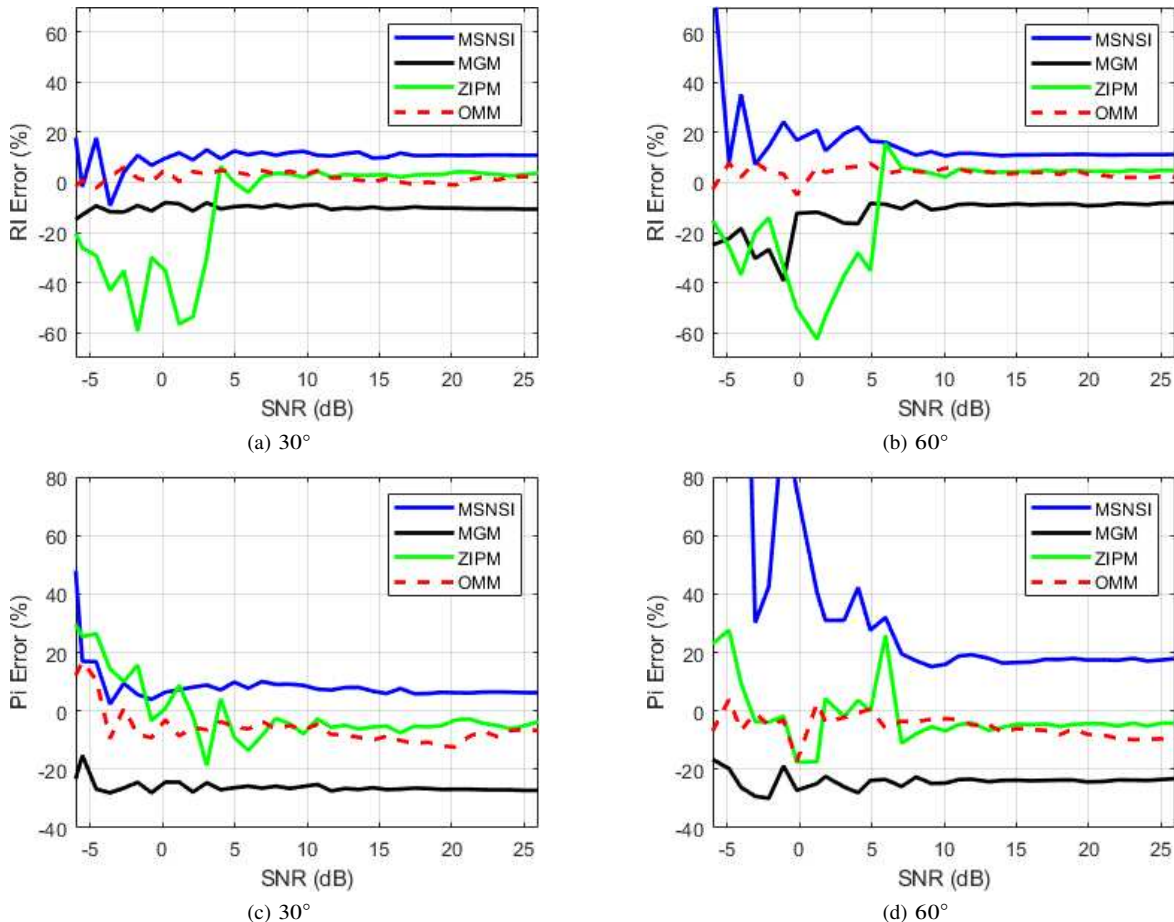
Fig. 14. PI and RI statistics for simulated carotid artery data using insonation angles of 30° and 60° across a range of SNR values.
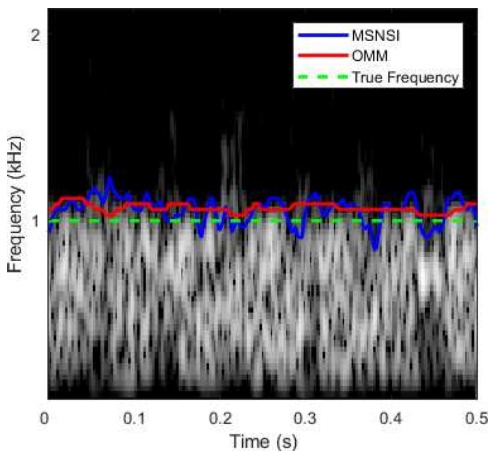

Fig. 15. Doppler spectrogram with estimated OMM and MSNSI MFEs using data from phantom producing 0.4 m/s flowrate. Displayed using dynamic range of 40 dB.

C. In-Vivo Data Results

The ability of the MFE estimation methods to perform under challenging conditions is evaluated further using in-vivo data. In addition to a variable SNR, in-vivo data includes erroneous contributions from, for example, tissue movement or other blood flows. The results presented here are for measurements of the aortic valve, in which a number of different features can be present [47]. Resulting envelopes, even in succeeding beats, can display high variability in size and shape.

The results using in-vivo data are presented in Table III. They demonstrate that, overall, the OMM method resulted in the lowest percentage error in terms of the total number of beats segmented; producing only 0.4% more beats than the true number of beats. The true number of beats was found by converting each recording into a spectrogram and counting the total number of whole beats present; data in which the total number of beats was hard to distinguish were removed. A whole beat is identified using the start or end of the preceding or proceeding beats, respectively. This allowed the number of beats within each recording to be compared to the number of beats extracted using each MFE method. The number of beats extracted for each MFE estimation method was then summed for all recordings giving a total number of overestimated and underestimated beats; the results are given in Table III. These values demonstrate that despite the OMM method percentage error being positive, this method resulted in the least number of overestimations. The OMM method also resulted in the least number of underestimations missing 0.8% of beats, compared to 5.8% missed by the next best-performing method, MSNSI.

The overestimation results in Table III illustrate that beat segmentation can result in beats incorrectly being segmented

TABLE III
NUMBER OF BEATS SEGMENTED USING EACH MFE METHOD

	OMM	MSNSI	MGM	ZIPM
Beats Segmented	7,908	7,613	7,677	7,491
Percentage Error[1] (%)	0.4	-3.4	-2.5	-4.9
Total Overestimations[2]	100	181	322	117
Total Underestimations[3]	69	445	522	503

(1) Percentage error of number of beats segmented with respect to true number.
(2) Summation of overestimated number of beats segmented from each recording.
(3) Summation of underestimated number of beats segmented from each recording.

TABLE IV
SEGMENTATION PERFORMANCE USING EACH METHOD ON SAMPLE OF IN-VIVO DATA

	OMM	MSNSI	MGM	ZIPM
True Positives (%)	97.8	89.6	64.6	89.6
False Negatives (%)	2.2	10.4	35.4	10.4
False Positives (%)	0.4	1.4	4.2	1.2

from the data; this is in response to erroneous signals or noise. The accuracies associated with performing beat segmentation using each of the MFE methods were further investigated using a sample of the in-vivo data.

A sample size of approximately 12% was used. The sample was attained by using the first four seconds of each of the 229 recordings. The extracted envelope and associated beat timing indices were generated for each audio sample and for each MFE method. Fig. 16 provides an example of this for the OMM and MGM envelope. This data allowed the number of false positives (a beat incorrectly segmented, or detected in the audio sample where there was no actual beat), false negatives (a beat present in the audio sample but not detected) and true positives (a beat existing in an audio sample was correctly detected) to be found . In Fig. 16, the OMM MFE resulted in four true positives, and the MGM MFE resulted in two false positives, one true positive and one false negative. The false positives occur due to the start of systole being incorrectly estimated for the second beat. This is due to there being

multiple narrow peaks in the systolic portion of this beat. The false negative occurred due to the final systolic peak not being preserved and therefore identified in the LPF MFE, resulting in the end of the fourth beat not being found. The results from the sample analysis are shown in Table IV.

Table IV illustrates that OMM resulted in the highest percentage of true positives, segmenting 97.8% of beats correctly; comparatively MSNSI and ZIPM both resulted in 89.6% of beats being correctly segmented. Use of the OMM method also resulted in the lowest percentage of false negatives and false positives, which is in line with the overestimations and underestimations in beat numbers given in Table III.

To evaluate the applicability of the proposed MFE and beat segmentation method for real-time applications, the time taken to run both algorithms for the in-vivo data was recorded. This was done using an Acer G9-592, with an i5-6300HQ CPU 2.3 GHz processor and 8 GB ram. The total processing time was 963 seconds, which corresponds to 0.12s per beat; accommodating a hypothetical maximum heart rate of up to 490 bpm for real-time applications.

Finally, a series of paired t-tests were performed on the results presented in Table III to confirm the differences in performance. The beat segmentation performance of the OMM method was compared to the remaining three MFE estimation methods independently. The resulting p-values for this analysis are very small ($3 \times 10^{-5}, 1 \times 10^{-3}$ and 4×10^{-14} for the MSNSI, MGM and ZIPM methods respectively), confirming the observed difference in performances was not random.

VI. DISCUSSION

A series of metrics and scenarios have been analysed to provide an in-depth comparison of the investigated MFE estimation methods. Metrics include STD, correlation and waveform indices. These were used to analyse the ability of the proposed method to extract representative Doppler profiles, from which shape information can be found or further beat segmentation performed.

The implementation of the methods remained constant for each data set apart from the case of ZIPM, for which this was not possible. This approach simulates real-world, automatic
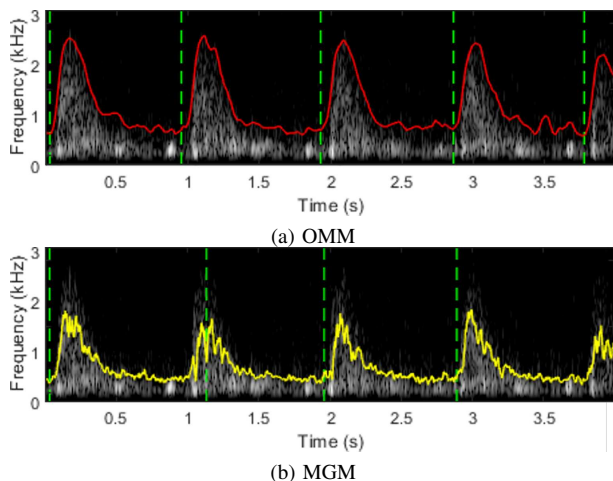

Fig. 16. Example of in-vivo data containing four whole beats with OMM and MGM MFEs and associated segmented beats, where the green dash indicates the start or ends of identified beats. In this case, OMM segmented four true positives, and MGM segmented two false positives, one true positive and one false negative. Using the OMM MFE, SNR was measured to be 15 dB.

application where true maximum velocities are unknown, or for research scenarios where datasets exhibit high variability (e.g., SNR and flow rates) and thus it is impractical to adjust the implementation of the methods. In certain other applications, for example, where maximum velocities of interest are more restricted, the methods could be tuned to give better performance (e.g., restricting image size for image-processing methods, or adjusting cut-off frequencies to improve the performance of IPS methods), however, this was beyond the scope of the presented work.

A. Envelope extraction using the Doppler Audio Signal

In the proposed method, the Doppler audio is used to form a spectrogram and from that an image. Thus the parameters used for generation of the spectrogram images are explicitly defined as discussed in Section IV. As described, the applied morphological operations are designed with respect to the resulting pixel resolution of these images. In contrast, the values of the parameters used to generate the images collected from an ultrasound machine are not known, and are device and user-specific. Variations and limitations between machines in this regard include screen refresh rates, spectrogram parameters, contrast, pixel resolution, zoom and image thresholding. The variations are in part due to the processing required to provide spectrograms as a form of visual feedback. In contrast, Doppler audio tends to naturally occur within a person's hearing range, allowing sonographers to use the audio feedback to guide probe position during measurements. This means that audio requires less processing prior to being used as a form of feedback in comparison to spectrogram images. The process of sampling audio is relatively straightforward and can be performed using basic hardware (e.g., a laptop). Considering this, implementing an image-processing MFE approach using the Doppler audio signal presents a number of advantages.

For this work, no specific standards with respect to streaming audio from commercial ultrasound machines could be found. The maximum Doppler frequencies, sample rate of any captured audio and the number of channels should, therefore, be considered prior to applying the proposed method. Fortunately, in many applications, Doppler signals are limited to relatively low frequencies and do not require high streaming standards.

B. Envelope Estimation with Decreasing SNR

The performance of each MFE estimation method was evaluated across a range of SNR values using both simulated and flow phantom data. In each case, SNR was estimated using (2), which provides a consistent means of comparing each method. This approach has been used in previous studies as it allows the noise to be quantified in real-world measurements [17], however, can give negative estimates in low SNR conditions. This is illustrated in Fig. 4, in which the Doppler profile is visually discernible at an SNR of -3dB. Evaluations have included such low SNRs to demonstrate the stability of the OMM method, and its potential to be used in automatic research or monitoring scenarios where noise conditions can vary. In terms of bias,

no MFE method consistently outperformed across the two data sets. Nonetheless, OMM typically achieved the lowest bias at lower SNRs (e.g., below 5 dB). It can be seen that unlike the other MFE methods, OMM exhibits decreasing bias with decreased SNR. This is due to the automatic thresholding used by OMM, which does not take into account spectral broadening. As more noise is introduced, the lower level spectral broadening is masked and the estimated maximum frequency is closer to the true value.

The OMM method produced very stable results across the SNR range with respect to the simulation correlation statistics (Fig. 12) and STD statistics for both the simulated and phantom data (Fig. 10 and Table II respectively). This is particularly evident in the correlation data, where the OMM method achieves a correlation greater than 95% at -6dB for both insonation angles.

The IPS methods typically exhibited more erratic behaviour than the image-processing methods. This is due to the fact that IPS methods require the IPS to exhibit its characteristic shape in order to accurately estimate maximum frequency points. This condition is met less consistently (for example, the IPS knee becomes less defined, and the transition from signal to noise more gradual) as SNR deteriorates and the measurements exhibit signal loss and increased variance. The MSNSI method compensates for this by employing only time points with adequate signal strength and then using interpolation and smoothing. If a portion greater than 0.1s with poor signal strength is identified, that region is set to zero. This is useful in measurements where flow discontinuities occur, in such cases the IPS curve would divert far from its characteristic shape and result in very poor maximum frequency estimations. The OMM method does not include any equivalent conditions, however, given that a global threshold is used to generate the binary images, small discontinuities do not result in incorrectly identified signal contributions. In such cases, the MFE is set to the minimum frequency bin in which flow signal can be detected. If no flow were present at all in a section of processed audio, the OMM method would be unable to detect this, and the resulting MFE would be erratic. The in-vivo data includes a large variety of waveforms and signal qualities, however, specific analysis of how each method performs in response to flow discontinuities was not performed and was beyond the scope of this investigation.

At a certain point, the MSNSI power threshold condition becomes detrimental as more of the envelope is set to zero. This begins to have an effect at SNRs below 10dB, this can be seen in Fig. 11, where regions of slow diastolic flow with lower spectral power have been set to 0. As SNR reduces further, the stable performance of MSNSI begins to become more erratic. Overall, the MSNSI method performed better despite MGM producing lower bias values than MSNSI at very high SNRs. This was found to be due to the MGM method performing very poorly during the weaker, diastolic portion of the signal.

The ZIPM method produced stable results at SNRs greater than 5dB but deteriorated quickly at lower SNRs. As described in Section IV-C, a dynamic range is chosen for the images processed using this method. This dynamic range dictates how successful proceeding thresholding is; as this is fixed,

at a certain SNR the signal can no longer be easily distinguished, and the method's performance quickly deteriorates. The dynamic range chosen to display the ZIPM images was chosen based on its performance with respect to the calculated statistics. Choosing the best dynamic range can be challenging when implementing ZIPM for new data. This was found to be the case using the in-vivo data, in which a dynamic range much larger than that used for the simulated and phantom data was required for good performance, and which is discussed further in Section VI-E. The dynamic range used for the ZIPM images meant only the strongest portion of the signal was visible (which occurs at the maximum velocity). Consequently, this meant the addition of noise had no effect on the binary image across a large range of the SNRs used. Additionally, the diastolic portion of the simulated femoral data could not be captured. The combination of this factor and slight overestimations with respect to maximum velocity during the systolic portion resulted in very low bias values, but less accurate STD and correlation values. ZIPM was able to produce good RI and PI results, this is partly due to the simulated carotid artery being more consistent. These results are discussed further in Section VI-D.

C. Envelope Estimation with Increasing Insonation Angle

The inherent properties of Doppler ultrasound systems give rise to a phenomenon known as intrinsic spectral broadening, which manifests as a blurring of the Doppler spectrum. A moving target, when measured using Doppler ultrasound, results in spectral content with a range of frequency shifts (and not one singular value). Blood contains many moving targets that contribute to the measured Doppler signal and result in a smearing of the frequency spectrum [1]. The presence of spectral broadening is attributed to two contributions referred to as local geometric broadening and transit-time broadening [48]. The degree of this effect increases with the insonation angle.

Simulated data was generated for insonation angles of 30°, and 60°. This allowed the effect of spectral broadening with respect to MFE estimation performance to be investigated. The bias, STD and correlation statistics show that typically the 60° simulated data resulted in deteriorated performance for all MFE methods. In the case of ZIPM, the increased insonation angle resulted in a lower bias. This was due to the combination of increased overestimation during systole, and underestimation during diastole as discussed in Section VI-B. The ZIPM envelope deviates further from the true envelope within the 60° data, which is illustrated from the STD results.

As discussed in Section VI-B, OMM exhibits increased bias at higher SNRs due to spectral broadening. This is more evident in the 60° data as higher insonation angles result in increased levels of spectral broadening. Use of metrics derived from MFEs, such as peak systole, should keep such effects in consideration.

The OMM method was able to generate highly correlated envelopes at low SNR values for both insonation angles. This means that despite spectral broadening, accurate MFE shape can still be extracted allowing successful beat segmentation or

accurate waveform features to be obtained. This is illustrated by the RI and PI statistics, which remain on average below 10% for the OMM method, for both angles and low SNRs. OMM and MSNSI resulted in similar absolute PI error at high SNRs for 30°. Increasing the insonation angle resulted in an absolute error increase of 47% and 185% for OMM and MSNSI respectively. OMM achieved a PI error of -10% for the 60° data, illustrating its potential use for such applications.

D. PI and RI Estimation

Features can be extracted from MFEs to provide additional means of analysing blood flow. The ability to extract two popular waveform indices, PI and RI, were investigated using each MFE estimation method. These results, shown in Fig. 14, illustrate that typically PI error was greater than RI error. Through inspecting the corresponding MFEs, it was found that performance was similar to that exhibited in the simulated femoral data. The OMM and MSNSI methods both produced envelopes with low bias. As bias is estimated from each time point, this corresponded to overall good estimates of the envelope mean. However, it was found that MSNSI overestimated peak systole, and increasingly so with SNRs below approximately 5 dB. This results in an overestimation of PI and RI values. Conversely, any inaccuracies in MFE estimation are more consistent across the whole MFE for image-processing methods. This results in more accurate PI and RI estimation. MGM performed similarly to MSNSI, however, underestimated peak systole resulting in negative PI and RI error.

Considering (3) and (4) and the more consistent M values, inaccurate S values are more detrimental for PI estimates. Furthermore, as discussed in Section VI-B, the MSNSI method results in more erratic behaviour at lower SNRs and includes a condition that can set portions of the MFE to 0. This increases the likelihood of D_{min} being smaller than D_{end}, and will further detrimentally affect estimates of PI.

It can be seen from Fig 14, that ZIPM begins to deteriorate below approximately 5 dB; this is consistent with the bias and STD results in Section V-A. As indicated by the correlation statistics in this Section, the ZIPM MFE rapidly deviates from the true MFE shape. This results in D_{end} increasing relative to S, and estimates of RI decreasing. The whole MFE increases, and although becomes far from the true MFE, does not result in huge RI and PI errors. Comparatively, the MSNSI envelopes resulted in worse PI and RI errors at low SNR, despite them overall being closer in shape to the true MFE. These observations highlight the need to consider different metrics when assessing MFE performance.

E. Beat Segmentation Performance

The ability to segment beats is essential for automatically extracting and monitoring beat specific measurements, like those discussed in the previous section. It allows for measurement averaging, preventing the practice of calculating values from representative beats, a process which may be a significant factor in test-retest variability [49]. Robust averaging has been shown to be clinically advantageous in certain applications, for

example, resynchronising pacemakers [9]–[11]. Furthermore, it makes analysis of larger datasets more feasible, which would be clinically desirable [50], and could enable research ventures that were previously deemed too time-consuming.

In this study, the ability to perform successful beat segmentation was investigated using a large dataset of in-vivo measurements. These measurements inevitably contain more artefacts than the simulated and phantom data. The measured signals include contributions from tissue movements and erroneous blood flow signals from nearby vessels. Other signals, such as valve clicks, can be present as well as variations in noise due to differences in transducer and tissue coupling and signals due to the transducer moving.

The results demonstrate that combining OMM with the described beat segmentation method can result in a high percentage of beats being correctly segmented, with the OMM method segmenting 8.2% more beats correctly than the next best performing method, MSNSI. Crucially, the sample test indicated that very few false positives were identified using OMM. This is a significant result of this research, as this characteristic is vital for applications which use processed beats to identify abnormalities in measurements, identify certain traits or perform classification tasks (such as classifying heart disease [51]). The difference in performance with respect to true positive and true negatives could be of particular significance when monitoring patients with challenging recordings such as weak cardiac output. The design and testing of the beat segmentation method has been limited to Doppler measurements from the aortic valve. This included data with a wide range of Doppler profiles, including ones far from their characteristic shape (e.g., high-end diastolic velocities). Considering this, the method is expected to also perform well using Doppler measurements from other locations (for example, from the carotid artery), however, this has not been confirmed.

In real-world applications, an automatic method needs to operate at sufficient speeds to extract the envelope, perform beat segmentation and extract information. The proposed method was found to take on average 0.12s to extract a segmented beat MFE, which provides 0.15s to extract additional information for a heart rate of 220 bpm. This illustrates that the proposed method could be implemented in real-world applications. Furthermore, the method requires only the MFE to function. This means no additional hardware is required and thus can remain low cost, fast and highly portable. Combining OMM and the proposed beat segmentation software allows real-time, continuous monitoring of a person's blood flow with live cardiac cycle analysis.

It was found that despite the good performance exhibited by ZIPM with respect to the simulation and phantom data, a much higher dynamic range was required to generate the images used in the in-vivo data. The low dynamic range used for the simulated and phantom data allowed the signal to be clearly defined (as shown in Fig. 8), however, the in-vivo data contains erroneous signals and variable SNR, preventing such a low dynamic range from being used. The need to select an appropriate dynamic range value for particular datasets stopped the ZIPM method from being truly automatic within this study.

VII. Conclusion

A new MFE estimation method (OMM) and a new beat segmentation method have been proposed in this work. The methods are fully automatic, can be implemented in a real-time manner and only require the Doppler audio signal as an input. The performance of OMM has been systematically evaluated for a wide range of signal qualities using simulated data, phantom data and in-vivo data. The performance has been compared with three other state of the art MFE estimation methods.

It was demonstrated that the proposed OMM method reliably produced envelopes suitable for further beat segmentation. Across a wide SNR range, the OMM method consistently produced the most stable envelopes with good correlation to the true shape. This was further demonstrated using in-vivo data, where it resulted in 8.2% more beats being correctly segmented in comparison to the next best performing method. This is a significant characteristic of the method and demonstrates its potential application for monitoring in clinical scenarios, and automatic processing of large datasets for research purposes.

References

[1] D. Evans, W. McDicken, R. Skidmore, and J. Woodcock, *Doppler Ultrasound; Physics, Instrumentation and Clinical Applications*, 2000.

[2] E. G. Grant, C. B. Benson, G. L. Moneta, A. V. Alexandrov, J. D. Baker, E. I. Bluth, B. A. Carroll, M. Eliasziw, J. Gocke, B. S. Hertzberg, S. Katarick, L. Needleman, J. Pellerito, J. F. Polak, K. S. Rholl, D. L. Wooster, and E. Zierler, "Carotid artery stenosis: grayscale and Doppler ultrasound diagnosis-society of radiologists in ultrasound consensus conference." in *Ultrasound quarterly*, 2003.

[3] J. Golledge, M. Ellis, T. Sabharwal, T. Sikdar, A. H. Davies, and R. M. Greenhalgh, "Selection of patients for carotid endarterectomy," *Journal of Vascular Surgery*, vol. 30, no. 1, pp. 122–130, 1999.

[4] A. T. Papageorghiou, C. K. Yu, S. Cicero, S. Bower, and K. H. Nicolaides, "Second-trimester uterine artery Doppler screening in unselected populations: A review," *Journal of Maternal-Fetal and Neonatal Medicine*, vol. 12, no. 2, pp. 78–88, 2002.

[5] L. L. Huntsman, D. K. Stewart, S. R. Barnes, S. B. Franklin, J. S. Colocousis, and E. A. Hessel, "Noninvasive Doppler determination of cardiac output in man. Clinical validation." *Circulation*, no. 3, pp. 593–602.

[6] R. A. Phillips, S. G. Hood, B. M. Jacobson, M. J. West, L. Wan, and C. N. May, "Pulmonary artery catheter (PAC) accuracy and efficacy compared with flow probe and transcutaneous doppler (USCOM): An ovine cardiac output validation," *Critical Care Research and Practice*, vol. 2012, 2012.

[7] F. Beltramo, J. Menteer, A. Razavi, R. G. Khemani, J. Szmuszkovicz, C. J. L. Newth, and P. A. Ross, "Validation of an Ultrasound Cardiac Output Monitor as a Bedside Tool for Pediatric Patients," *Pediatric Cardiology*, vol. 37, no. 1, pp. 177–183, 2016.

[8] E. Y. Lui, A. H. Steinman, R. S. Cobbold, and K. W. Johnston, "Human factors as a source of error in peak Doppler velocity measurement," *Journal of Vascular Surgery*, vol. 42, no. 5, pp. 3–6, 2005.

[9] S. M. Sohaib, Z. I. Whinnett, K. A. Ellenbogen, C. Stellbrink, T. A. Quinn, M. D. Bogaard, P. Bordachar, B. M. Van Gelder, I. E. Van Geldorp, C. Linde, M. Meine, F. W. Prinzen, R. G. Turcott, H. M. Spotnitz, D. Wichterle, and D. P. Francis, "Cardiac resynchronisation therapy optimisation strategies: Systematic classification, detailed analysis, minimum standards and a roadmap for development and testing," *International Journal of Cardiology*, no. 2, pp. 118–131.

[10] D. P. Francis, "How to reliably deliver narrow individual-patient error bars for optimization of pacemaker AV or VV delay using a 'pick-the-highest' strategy with haemodynamic measurements," *International Journal of Cardiology*, no. 3, pp. 221–225.

[11] P. A. Pabari, K. Willson, B. Stegemann, I. E. Van Geldorp, A. Kyriacou, M. Moraldo, J. Mayet, A. D. Hughes, and D. P. Francis, "When is an optimization not an optimization? Evaluation of clinical implications of information content (signal-to-noise ratio) in optimization of cardiac resynchronization therapy, and how to measure and maximize it," *Heart Failure Reviews*, vol. 16, no. 3, pp. 277–290, 2011.

[12] A. H. Steinman, J. Tavakkoli, J. G. Myers, R. S. C. Cobbold, and K. W. Johnston, "Sources of error in maximum velocity estimation using linear phased-array Doppler systems with steady flow," *Ultrasound in Medicine and Biology*, vol. 27, no. 5, pp. 655–664, 2001.

[13] T. D'Alessio, "Objective algorithm for maximum frequency estimation in Doppler spectral analysers," *Medical & Biological Engineering & Computing*, 1985.

[14] L. Y. L. Mo, L. C. Yun, and R. S. Cobbold, "Comparison of four digital maximum frequency estimators for Doppler ultrasound," *Ultrasound in Medicine and Biology*, vol. 14, no. 5, pp. 355–363, 1988.

[15] R. Moraes, N. Aydin, and D. Evans, "The performance of three maximum frequency envelope detection algorithms for Doppler signals," *Journal of Vascular Investigation*, no. 3, pp. 126–134.

[16] K. Marasek and A. Nowicki, "Comparison of the performance of three maximum Doppler frequency estimators coupled with different spectral estimation methods," *Ultrasound in Medicine and Biology*, vol. 20, no. 7, pp. 629–638, 1994.

[17] A. Kathpalia, Y. Karabiyik, S. H. Eik-nes, E. Tegnander, I. K. Ekroll, G. Kiss, and H. Torp, "Adaptive spectral envelope estimation for Doppler ultrasound," *IEEE Transactions on Ultrasonics, Ferroelectrics, and Frequency Control*, vol. 63, no. 11, pp. 1825–1838, 2016.

[18] J. Tschirren, R. M. Lauer, and M. Sonka, "Automated analysis of Doppler ultrasound velocity flow diagrams." *IEEE Trans Med Imaging*, 2001.

[19] O. Shechner, M. Scheinowid, M. S. Feinberg, and H. Greenspan, "Automated method for Doppler echocardiography image analysis," *Proc. 23rd IEEE Convent. Elect. Electron. Eng. Israel*, pp. 177–180, 2004.

[20] O. Shechner, M. Sheinovitz, M. Feinberg, and H. Greenspan, "Image analysis of Doppler echocardiography for patients with atrial fibrillation," in *2004 2nd IEEE International Symposium on Biomedical Imaging: Macro to Nano*, 2004.

[21] H. Greenspan, O. Shechner, M. Scheinowitz, and M. S. Feinberg, "Doppler echocardiography flow-velocity image analysis for patients with atrial fibrillation," *Ultrasound in Medicine and Biology*, vol. 31, no. 8, pp. 1031–1040, 2005.

[22] V. Magagnin, L. Delfino, S. Cerutti, M. Turiel, and E. G. Caiani, "Nearly automated analysis of coronary Doppler flow velocity from transthoracic ultrasound images: Validation with manual tracings," *Medical and Biological Engineering and Computing*, vol. 45, no. 5, pp. 483–493, 2007.

[23] T. Syeda-Mahmood, P. Turaga, D. Beymer, F. Wang, A. Amir, H. Greenspan, and K. Pohl, "Shape-based similarity retrieval of Doppler images for clinical decision support," *Proceedings of the IEEE Computer Society Conference on Computer Vision and Pattern Recognition*, pp. 855–862, 2010.

[24] M. Zolgharni, N. M. Dhutia, G. D. Cole, M. R. Bahmanyar, S. Jones, S. M. A. Sohaib, S. B. Tai, K. Willson, J. A. Finegold, and D. P. Francis, "Automated aortic Doppler flow tracing for reproducible research and clinical measurements," *IEEE Transactions on Medical Imaging*, vol. 33, no. 5, pp. 1071–1082, 2014.

[25] P. Gifani, H. Behnam, A. Shalbaf, and Z. A. Sani, "Automatic detection of end-diastole and end-systole from echocardiography images using manifold learning," *Physiological Measurement*, vol. 31, no. 9, pp. 1091–1103, 2010.

[26] S. Brekke, E. Tegnander, H. G. Torp, and S. H. Eik-Nes, "Tissue Doppler gated (TDOG) dynamic three-dimensional ultrasound imaging of the fetal heart," *Ultrasound in Obstetrics and Gynecology*, vol. 24, no. 2, pp. 192–198, 2004.

[27] N. Otsu, "A threshold selection method from gray-level histograms," *IEEE Transactions on Systems, Man, and Cybernetics*, 1979.

[28] D. Maulik, "Spectral Doppler: Basic principles and instrumentation," *Doppler Ultrasound in Obstetrics and Gynecology: 2nd Revised and Enlarged Edition*, pp. 19–34, 2005.

[29] R. W. Gill, "Measurement of blood flow by ultrasound: Accuracy and sources of error," *Ultrasound in Medicine and Biology*, vol. 11, no. 4, pp. 625–641, 1985.

[30] Y. Zhang, J. C. Cardoso, Y. Wang, P. J. Fish, C. A. Bastos, and W. Wang, "Time-scale removal of 'wall thump' in Doppler ultrasound signals: A simulation study," *IEEE Transactions on Ultrasonics, Ferroelectrics, and Frequency Control*, vol. 51, no. 9, pp. 1187–1192, 2004.

[31] P. Fish, *Physics and Instrumentation of Diagnostic Medical Ultrasound*. Chichester, Sussex: John Wiley & Sons, 1990.

[32] N. Biradar, M. L. Dewal, and M. K. Rohit, "Comparative analysis of despeckling filters for continuous wave Doppler images," *Biomedical Engineering Letters*, vol. 5, no. 1, pp. 33–44, 2015.

[33] J. Tchirren, R. M. Lauer, and M. Sonka, "Automated analysis of Doppler ultrasound velocity flow diagrams," vol. 23, no. 1, pp. 130–133, 2001.

[34] R. Strand, "Automatic flow tracking system and method," U.S. Patent 0137717, June 03, 2003.

[35] A. D. Jose and D. Collison, "The normal range and determinants of the intrinsic heart rate in man," *Cardiovascular Research*, vol. 4, no. 2, pp. 160–167, 1970.

[36] P. Vaitkus and R. Cobbold, "A comparative study and assessment of Doppler ultrasound spectral estimation techniques part I: Estimation methods," *Ultrasound in Medicine and Biology*, no. 8, pp. 661–672.

[37] L. Y. Mo and R. Cobbold, "'Speckle' in continuous wave Doppler ultrasound spectra: A simulation study," *IEEE Transactions on Ultrasonics, Ferroelectrics and Frequency Control*, no. 6, pp. 747–753.

[38] G. H. Van Leeuwen, A. P. Hoeks, and R. S. Reneman, "Simulation of real-time frequency estimators for pulsed Doppler systems," *Ultrasonic Imaging*, 1986.

[39] J. A. Jensen and N. B. Svendsen, "Calculation of pressure fields from arbitrarily shaped, apodized, and excited ultrasound transducers," *IEEE Transactions on Ultrasonics, Ferroelectrics, and Frequency Control*, 1992.

[40] J. A. Jensen, "Field: A program for simulating ultrasound Systems," *Medical and Biological Engineering and Computing*, no. 1, pp. 351–352.

[41] ——, "Focusing along the flow direction I : Theory and simulation," *IEEE Transactions on Ultrasonics, Ferroelectrics, and Frequency Control*, 2003.

[42] J. A. Jensen, S. Member, and R. Bjerngaard, "Along the flow direction II : Experimental investigation," *Development*, vol. 50, no. 7, pp. 873–880, 2003.

[43] J. A. Jensen, "Simulation of advanced ultrasound systems using Field II," *2004 2nd IEEE International Symposium on Biomedical Imaging: Macro to Nano (IEEE Cat No. 04EX821)*, pp. 636–639.

[44] J. R. Womersley, "Oscillatory flow in arteries: The constrained elastic tube as a model of arterial flow and pulse transmission," *Physics in Medicine and Biology*, 1957.

[45] J. A. Jensen, "Calculation of pulsed wave phantom data for arteria femoralis," 2019. [Online]. Available: https://field-ii.dk/examples/pw_example/example_pw_phantom.html

[46] I. T. Gabe, J. H. Gault, J. Ross, D. T. Mason, C. J. Mills, J. P. Schillingford, and E. Braunwald, "Measurement of instantaneous blood flow velocity and pressure in conscious man with a catheter-tip velocity probe." *Circulation*, 1969.

[47] L. A. H. Critchley and L. Huang, "USCOM - Window to the circulation: Utility of supra-sternal Doppler in an elderly anaesthetized patient for a robotic cystectomy," *Journal of Clinical Monitoring and Computing*, vol. 28, no. 1, pp. 83–93, 2014.

[48] G. Guidi, C. Licciardello, and S. Falteri, "Intrinsic spectral broadening (ISB) in ultrasound Doppler as a combination of transit time and local geometrical broadening," *Ultrasound in Medicine and Biology*, vol. 26, no. 5, pp. 853–862, 2000.

[49] J. A. Finegold, C. H. Manisty, F. Cecaro, N. Sutaria, J. Mayet, and D. P. Francis, "Choosing between velocity-time-integral ratio and peak velocity ratio for calculation of the dimensionless index (or aortic valve area) in serial follow-up of aortic stenosis," *International Journal of Cardiology*, no. 4, pp. 1524–1531.

[50] C. H. Manisty, A. Al-Hussaini, B. Unsworth, R. Baruah, P. A. Pabari, J. Mayet, A. D. Hughes, Z. I. Whinnett, and D. P. Francis, "The acute effects of changes to AV delay on BP and stroke volume potential implications for design of pacemaker optimization protocols," *Circulation: Arrhythmia and Electrophysiology*, vol. 5, no. 1, pp. 122–130, 2012.

[51] E. Çomak, A. Arslan, and I. Türkoğlu, "A decision support system based on support vector machines for diagnosis of the heart valve diseases," *Computers in Biology and Medicine*, vol. 37, no. 1, pp. 21–27, 2007.